ORIGINAL PAPER

Trace-element partitioning between gregoryite, nyerereite, and natrocarbonatite melt: implications for natrocarbonatite evolution

Céline Baudouin[1] · **Lydéric France**[2,3]

Abstract

Trace-element partitioning between gregoryite, nyerereite, and natrocarbonatite melt is primordial for understanding trace-element distribution and fractionation in alkali-rich carbonatites. However, trace-element data are scarce for gregoryite and nyerereite. Here, we provide the first partition coefficients and lattice strain model parameters for trace-element partitioning between these carbonate minerals and natrocarbonatite at Oldoinyo Lengai (Tanzania). Nyerereite and gregoryite phenocrysts crystallize within a shallow magmatic reservoir (< 3 km depth, ~ 600 °C), and gregoryite continues to crystallize during magma ascent at lower pressures. At these low-temperature and pressure conditions, trace elements behave incompatibly in both gregoryite and nyerereite. Trace-element partitioning is characterized by a parabolic fit between the partition coefficients and ionic radii that is explained by a lattice strain model in which the site radius (r_0) decreases with increasing charge from $r_0^{1+} = 1.1$ Å to $r_0^{4+} = 0.75$ Å. We observed different partition coefficients in gregoryite (Ggy) and nyerereite (Nye): those in nyerereite are greater than those in gregoryite for REEs ($D_{Nd}^{Nye} = 0.58$ *vs.* $D_{Nd}^{Ggy} = 0.21$; $D_{La}^{Nye} = 0.27$ *vs.* $D_{La}^{Ggy} = 0.12$), Sr ($D_{Sr}^{Nye} = 0.92$ *vs.* $D_{Sr}^{Ggy} = 0.5$), Ba ($D_{Ba}^{Nye} = 0.22$ *vs.* $D_{Ba}^{Ggy} = 0.1$), and Rb ($D_{Rb}^{Nye} = 0.35$ *vs.* $D_{Rb}^{Ggy} = 0.26$), but lower for HFSEs (e.g., $D_{Hf}^{Nye} = 0.13$ *vs.* $D_{Hf}^{Ggy} = 0.28$; $D_{Nb}^{Nye} = 0.02$ *vs.* $D_{Nb}^{Ggy} = 0.08$). Because all trace elements are incompatible, their concentrations increase in the melt during differentiation and the crystallization of both gregoryite and nyerereite. Due to their different partition coefficients, we can constrain the shallow crustal crystallization history of natrocarbonatite melts at Oldoinyo Lengai: the crystallization of roughly equal proportions of gregoryite and nyerereite can produce aphyric natrocarbonatite compositions from a typical natrocarbonatite composition. The late-stage crystallization of gregoryite alone during magmatic ascent and eruption can significantly impact the concentrations of key elements, such as increasing LREE contents and LREE/HFSE and LILE/HFSE ratios in the residual melt. Our results also highlight that natrocarbonatite melt crystallization during the 2019 eruption proceeded at temperatures from 600 °C to as low as 300 °C.

Keywords Natrocarbonatite · Partition coefficient · Oldoinyo Lengai · Carbonate minerals · Rare-earth elements · REE

✉ Céline Baudouin
celine.baudouin@sorbonne-universite.fr

[1] ISTeP-Earth Sciences Institute-CNRS-Sorbonne Université, 4 Pl. Jussieu, 75005 Paris, France

[2] Université de Lorraine, CNRS, CRPG, 54000 Vandoeuvre-les-Nancy, France

[3] Institut Universitaire de France (IUF), Paris, France

Introduction

Oldoinyo Lengai (OL) is an active carbonatite–nephelinite–phonolite volcano in northern Tanzania characterized by the unique occurrence of natrocarbonatite worldwide. The OL edifice is mainly composed of phonolite (60%) and nephelinite (35%), but only 5% natrocarbonatite (Klaudius and Keller 2006); the latter were likely present at OL since at least 11 ka (France et al. 2021). In the last century, eruptions at OL have been characterized by long periods of effusive natrocarbonatite eruptions and shorter periods of explosive alkaline–nephelinitic activity (Dawson et al. 1995; Keller et al. 2010). Although likely associated with magma

recharge events, the explosive phases do not significantly modify the geochemical composition of the carbonatite melt or of its associated gas emissions (Bosshard-Stadlin et al. 2014; Mollex et al. 2018).

Carbonatites are igneous rocks formed from carbonate-rich magmas and can be classified by their chemical compositions: calciocarbonatite, magnesiocarbonatite, and ferrocarbonatite. Natrocarbonatites are evolved carbonatite which are derived from calciocarbonatite compositions and present highly alkaline compositions (e.g., Zaitsev and Keller 2006; Weidendorfer et al. 2017; Yaxley et al. 2022). Whereas most carbonatites contain calcite or dolomite, natrocarbonatites contain gregoryite $(Na,K,Ca_x)_{2-x}(CO_3)$ and nyerereite $(Na,K)_2Ca(CO_3)_2$ phenocrysts with groundmass phases of Na-rich gregoryite, barian nyerereite, sylvite, fluorite, apatite, alabandite, and residual carbonate melt (e.g., Mitchell 2006). Aside from its occurrence in OL natrocarbonatites, nyerereite also occurs as inclusions in other carbonatites (Stoppa et al. 2009; Chen et al. 2013). Typical natrocarbonatites exhibit varying eruptive textures: highly porphyritic (75–80 vol.% phenocrysts), porphyritic (35–75 vol.% phenocrysts of which 26 vol.% are nyerereite, 22 vol.% are gregoryite, and 52 vol.% are groundmass), and groundmass-rich (< 35 vol.% phenocrysts) (Keller and Krafft 1990; Keller and Zaitsev 2012). This textural variety depends on the eruptive conditions and crystal–liquid fractionation during sub-aerial flow (e.g., Keller and Krafft 1990). Atypical natrocarbonatites are silicate-bearing (Dawson et al. 1996; Kervyn et al. 2008), sylvite-fluorite-bearing (Mitchell 2006), or residual aphyric natrocarbonatites (Keller and Krafft 1990).

Major- and trace-element concentrations in gregoryite and nyerereite have been documented in various natrocarbonatites (Zaitsev et al. 2009; Mitchell and Kamenetsky 2012). Previous geochemical analyses of phenocrysts indicate that nyerereite is richer in Sr (14,900–27,577 ppm), Ba (2,776–12,718 ppm), and rare-earth elements (REEs; $\sum REE = 880–1,018$ ppm), whereas gregoryite is rich in P (1.76–4.53 wt.% P_2O_5), V (22–31 ppm), and Li (119–241 ppm) (Mitchell and Kamenetsky 2012). Although previous studies focused on bulk rock (Keller and Krafft 1990; Peterson 1990; Keller and Zaitsev 2012) or mineral compositions (Keller and Spettel 1995; Zaitsev et al. 2009; Mitchell and Kamenetsky 2008, 2012), no data are available for trace-element partitioning between gregoryite, nyerereite, and carbonate melt. Nonetheless, elemental partitioning data are required to better understand the formation and evolution of natrocarbonatites, specifically the evolution of the residual melt during natrocarbonatite differentiation and the formation of REE-rich lithologies associated with carbonatites. Here, we present the first partition coefficients between gregoryite, nyerereite, and natrocarbonatite melt, and discuss the implications for natrocarbonatite differentiation.

Sampling and petrography

Molten natrocarbonatite lava was collected in 2019 from within the crater of OL following the sampling technique of Laxton (2020). Lava has been collected using a series of tensioned ropes and stainless-steel cups that were lowered onto the crater and submerged into natrocarbonatite liquid. Due to the hygroscopic nature of natrocarbonatite (Zaitsev and Keller 2006), rapidly air-quenched samples were packed in desiccant to preserve their pristine mineralogy and avoid alteration under atmospheric conditions.

We studied natrocarbonatite sample OL_06 (Laxton 2022), which contains prismatic nyerereite (25–27 vol.%, 0.2–1 mm), rounded gregoryite (22–27 vol.%, 0.2–1.5 mm)(Fig. 1), and 51 vol.% groundmass comprising gregoryite and nyerereite microcrysts, minor fluorite and sylvite, and large vesicles (11 vol.%, 0.5–1 mm) (Fig. A1). This sample (OL_06) is among the natrocarbonatites containing more gregoryite than nyerereite phenocrysts according to Laxton 2022 and has a high bulk P content. The modal composition of this sample is close to that of the average modal composition of the type porphyritic natrocarbonatite (Keller and Krafft 1990).

Analytical methods

We determined major and volatile element concentrations in gregoryite and nyerereite phenocrysts by electron microprobe analyses (Cameca SX100) at the University of Lorraine (France) using an accelerating voltage of 15 kV, a beam current of 5 nA, and a 20-μm-diameter beam. On-peak and background counting times were 10 s for all elements. We used wollastonite as a standard for Si and Ca, Al_2O_3 for Al, hematite for Fe, orthoclase for K, albite for Na, apatite for P and Cl, $SrSO_4$ for Sr and S, and topaz for F. X-ray maps were obtained on the same instrument with an accelerating voltage of 15 kV, a beam current of 50 nA, a focused beam, step sizes of 7–12 μm, and a dwell time of 100 ms. We calculated an average groundmass major-element composition from the mineral modal compositions (22% nyerereite and 27% gregoryite), and the bulk rock (OL_06, Table 1) and average mineral analyses. Bulk rock analysis and analytical method were presented by Laxton (2022). The calculated groundmass composition is within the range of natrocarbonatite (15.5 wt.% CaO and 35 wt.% Na_2O). Modal mineral proportions were determined from thin section observations by observation under the microscope and back-scattered electron petrography.

Mineral trace-element concentrations were determined by laser ablation inductively coupled mass spectrometry

Fig. 1 Backscattered electron image of natrocarbonatite sample OL_06 from Oldoinyo Lengai and chemical maps obtained by electron microprobe. Elemental concentrations are in wt. %
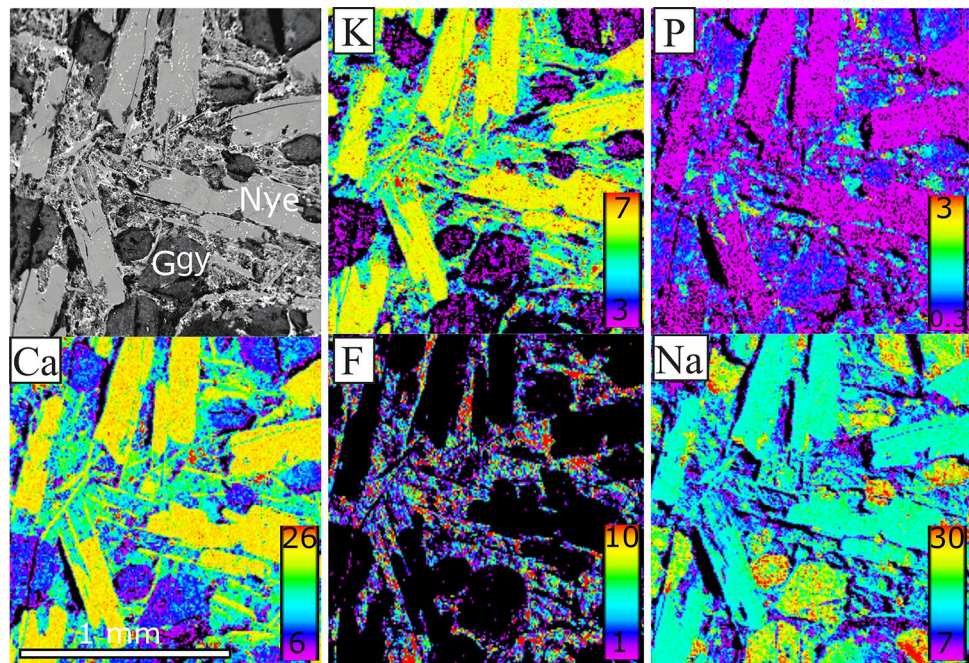
Table 1 Major-element compositions (wt.%) of the bulk rock OL_06 natrocarbonatite and gregoryite and nyerereite therein

	OL_06	Gregoryite avg	Gregoryite core	Gregoryite micro	Ggy SD	Nyerereite	Nye SD
SiO_2	0.31	0.74	1.51	0.33	0.35	0.04	0.06
Al_2O_3	0.01	0.02	0.01	0.06	0.02	n.a	n.a
Fe_2O_3	0.25	0.04	0.11	0.06	0.05	0.013	0.006
MnO	0.28	0.04	0.03	0.04	0.01	0.08	0.02
MgO	0.35	n.a	n.a	n.a	n.a	n.a	n.a
CaO	16.85	8.30	10.99	5.7	1.63	24.46	0.17
SrO	1.75	0.55	0.71	0.43	0.19	2.06	0.05
BaO	1.49	n.a	n.a	n.a	n.a	n.a	n.a
Na_2O	31.84	40.01	34.1	42.65	3.28	21.72	0.32
K_2O	6.21	2.43	3.32	1.5	0.57	7.82	0.09
P_2O_5	1.15	2.13	2.85	2.02	0.43	0.82	0.09
Cl	1.22	n.a	n.a	n.a	n.a	n.a	n.a
SO_3	2.69	0.95	1.75	0.73	0.34	1.03	0.17
F	1.98	n.a	n.a	n.a	n.a	n.a	n.a
CO_2	32.50	n.a	n.a	n.a	n.a	n.a	n.a
H_2O	1.12	n.a	n.a	n.a	n.a	n.a	n.a
$-O = F,Cl,(S)$	−1.11						
Total	98.89	55.41	55.34	53.48		58.39	

Gregoryite occurs as phenocrysts and microcrysts: average (avg) and core compositions are reported for phenocrysts, and microcrysts (micro) are reported separately, *n.a.* not analyzed, *SD* standard deviation

(LA-ICP-MS) at the Georessources Laboratory of the University of Lorraine using an AGILENT 7500 coupled with a GEOLAS Pro laser (193 nm). Laser beam diameters of 70 and 100 μm were used for mineral (gregoryite, $n = 43$; nyerereite, $n = 39$), and groundmass analyses ($n = 43$), respectively, with a laser repetition rate of 5 Hz and a laser fluence of 5 J cm^{-2}. These spot sizes were chosen as a compromise between signal intensity and the mineral sizes in the samples. The analysis time for each sample was 100 s, comprising 45 s of background measurement (laser off) and 55 s of analysis with the laser on. Trace-element concentrations were calibrated against NIST612

glass, and CaO (6.2–11.1 wt.% in gregoryite; 17 wt.% in groundmass) and Na_2O concentrations (24.0–24.4 wt.% in nyerereite) previously determined by electron microprobe were used as internal standards. The NIST610 standard was used as external standard. Detection limits for most trace elements were in the range 1–20 ppb. Tm, Yb, and Lu concentrations in minerals were slightly above the detection limits (Supplementary material). Standard errors were < 10% for most elements and around 7% for REEs (Supplementary material). We used Glitter (Griffin et al. 2008) to process the raw data files (signal intensity *vs.* time) and calculate trace-element concentrations, which allowed precise selection of blanks and signals, and rapid visualization of the intensity data. All data reported herein are from analyses of minerals free of inclusions or glass. Instrumental drift was compensated by the internal standard calculations using Glitter; no other drift corrections were performed.

Results

Natrocarbonatite composition

Natrocarbonatite lava OL_06 (Laxton 2022) is alkali-rich ($Na_2O + K_2O = 38$ wt.%) with high CaO (16.85 wt.%) and low SiO_2, TiO_2, Al_2O_3, MnO, and MgO contents (< 1 wt.% combined). The major- and trace-element concentrations in the studied sample (bulk rock) are relatively similar to those characterized for the type porphyritic natrocarbonatite (porphyritic carbonatite: 35–75 vol.% phenocrysts; Keller and Krafft 1990; Keller and Zaitsev 2012). Our sample had lower Cl (1.2 wt.%) and K_2O (6.2 wt.%) and higher Sr contents (13,600 ppm) relative to the type natrocarbonatite. OL_06 also has lower REE contents ($\sum REE = 930$ ppm) than the type natrocarbonatite ($\sum REE = 1,000$–1,700 ppm; Keller and Zaitsev 2012).

OL_06 shows distinct chemical characteristics compared to Si-rich, Cl-F-rich, and aphyric/residual natrocarbonatites. OL_06 contains less SiO_2 (0.3 wt.%) than Si-rich natrocarbonatites (1.2–3.5 wt.% SiO_2), less Cl and F (1.2 wt.% and 2.0 wt.%, respectively) than sylvite–fluorite microphenocryst-bearing natrocarbonatites, and less K_2O and Ba (6.2 wt.% and 13,000 ppm, respectively) than aphyric natrocarbonatites (9.1–9.6 wt.% K_2O, 19,400–20,000 ppm Ba). Overall, OL_06 is chemically classified as a natrocarbonatite (Fig. 2).

Nyerereite composition

Nyerereite phenocrysts exhibit little major-element chemical variations: 21.2–22.1 wt.% Na_2O, 24.1–24.7 wt.% CaO, 7.7–8.0 wt.% K_2O, and 0.70–1.24 wt.% SO_3 with

no significant intracrystal variations (Fig. 2). Large ion lithophile element (LILE) concentrations are high for Sr (14,110–22,700 ppm) and Ba (5,860–19,420 ppm), and low for Rb (109–258 ppm) (Fig. 3). Chondrite-normalized (denoted by the subscript 'N', chondrite values from McDonough and Sun 1995) light REE (LREE) concentrations ($La_N > 1,000$, $Sm_N > 20$) are high and display strong LREE to middle REE (MREE) fractionations (180–570 ppm La, $La_N/Sm_N = 40$–120). MREE contents are moderate (3–5 ppm Sm), and heavy REE (HREE) contents are low with high LREE/HREE fractionations (0.01–0.04 ppm Yb, $La_N/Yb_N = 6,200$–16,800) (Fig. 4). Nyerereites also have high concentrations of other trace elements (250–855 ppm Si, 345–990 ppm Mn, 20–170 ppm Li, 5–20 ppm V) and low concentrations of high field strength elements (HFSEs; 0.04–1.00 ppm Nb, < 0.01–0.07 ppm Zr, < 0.01–0.03 ppm Ta) (Table 2, supplementary material).

Gregoryite composition

Gregoryite phenocrysts have heterogeneous major-element compositions with variable Na and Ca contents (Table 1): 34.1–44.6 wt.% Na_2O, 5.7–11.0 wt.% CaO, 1.5–3.3 wt.% K_2O, 0.50–1.75 wt.% SO_3, and 1.5–2.8 wt.% P_2O_5. Similar major-element ranges were reported by Zaitsev et al. (2009) and Mitchell and Kamenetsky (2012). Microcrysts (< 100 μm) have low CaO (5.7–8.4 wt.%) and high Na_2O contents (38.8–44.6 wt.%), whereas phenocrysts (~ 500 μm) have higher CaO (8.35–11.00 wt.%) and lower Na_2O contents (34.1–38.6 wt.%). Gregoryite is poorer in some trace elements relative to nyerereite, particularly Sr (3,770–21,250 ppm), Ba (1,270–7,100 ppm), Rb (34–320 ppm), and LREEs (e.g., 45–310 ppm La) (Fig. 3). REE concentrations display relatively high LREE/MREE ratios ($La_N > 500$, $Sm_N > 1.2$, $La_N/Sm_N = 80$–130), moderate MREE contents (0.5–0.8 ppm Sm), low HREE contents (< 0.01–0.07 ppm Yb), and high LREE/HREE ratios ($La_N/Yb_N = 29,070$–11,140) (Fig. 4). Compared to nyerereite, gregoryite has higher concentrations of transition metals such as Mn (800–3000 ppm), V (64–340 ppm), Fe (30–1,800 ppm,), Mo (2–60 ppm), and HFSEs (0.2–3.0 ppm Nb, < 0.01–0.40 Zr, < 0.01–0.04 ppm Ta)(Table 2). Gregoryite also has high Li contents (75–820 ppm Li). Inter-phenocryst compositions are variable: small grains are enriched in Li, Sr, and Ba (Fig. 5), whereas some large grains have rims depleted in Li, Sr, and Ba relative to their cores.

Groundmass composition

Using mass-balance calculation based on modal mineral proportions, we defined the matrix major-element composition to be 14–19 wt.% CaO (average value at 17 wt.%), 32.5–35.0 wt.% Na_2O, 7.2–7.5 wt.% K_2O, 2.2 wt.% SrO (Table in supplementary material). Groundmass
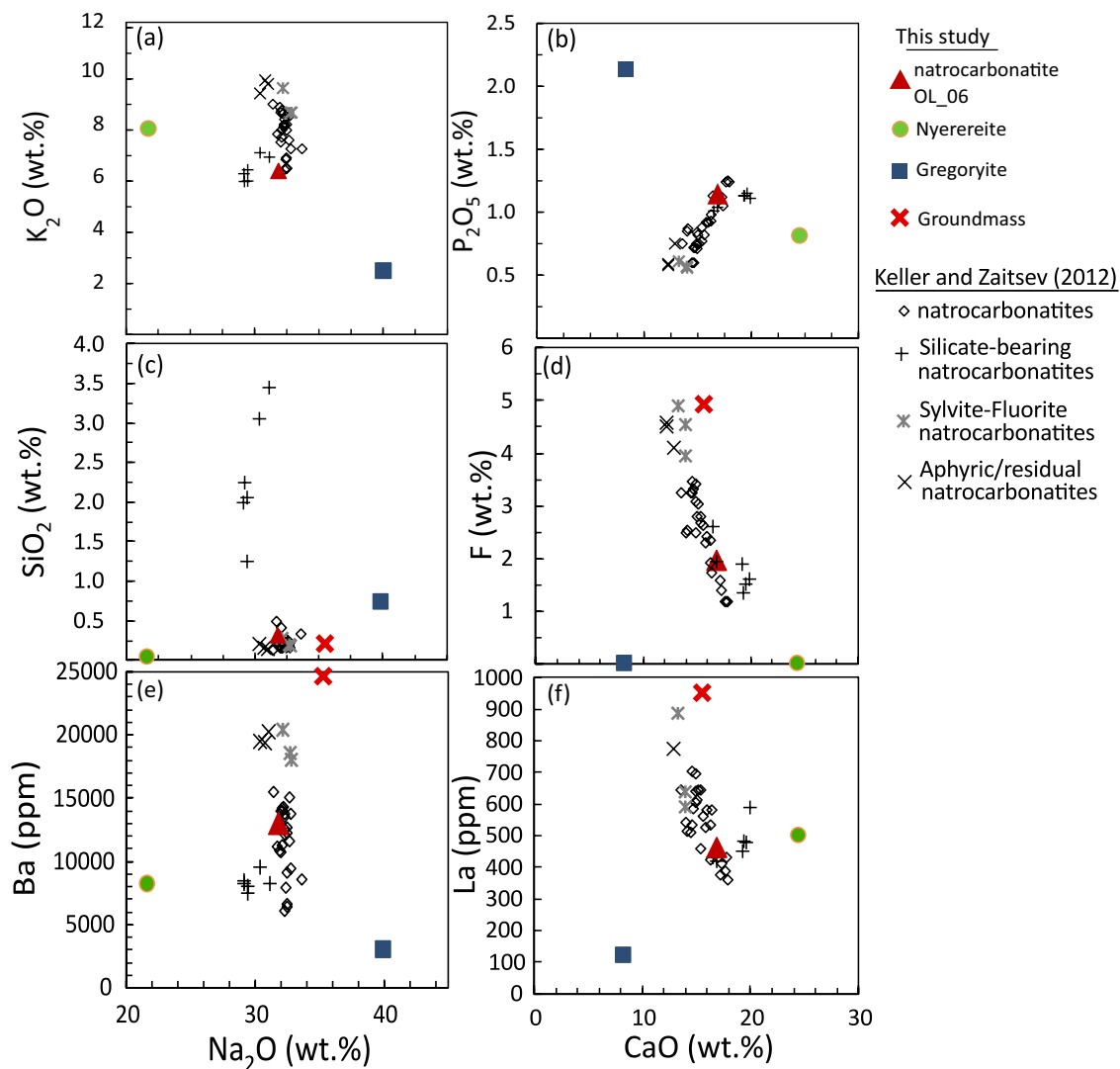
Fig. 2 Bulk rock compositions of different types of natrocarbonatites. Data from this study and Keller and Zaitsev (2012)
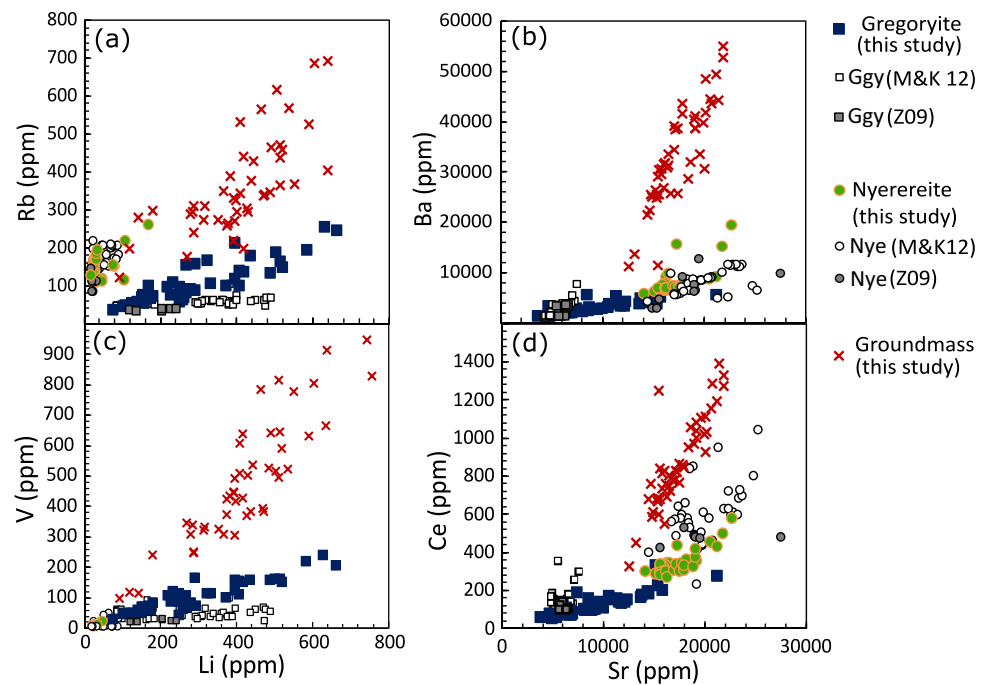
trace-element concentrations (e.g., 247–1,575 ppm La, $La_N/Yb_N = 4,400–22,000$) are higher than in the bulk OL_06 composition but similar to residual natrocarbonatites (Fig. 2) (Keller and Zaitsev 2012). Relative to all other natrocarbonatite types, the groundmass is enriched in LILEs (8,620–55,000 ppm Ba, 9,617–30,334 ppm Sr, 92–1,160 ppm Rb), transition metals (401–7,726 ppm Mn, 74–975 ppm V), and HFSEs (0.5–15.0 ppm U, 0.2–55.0 ppm Nb, 0.02–2.50 ppm Zr). The groundmass displays a small fractionation of Zr relative to Hf ($(Zr/Hf)_N = 0.1–3$) (Fig. 4, Table 2). LILE concentrations (i.e., Rb, Ba, and Sr) are positively correlated with La contents, but not Nb, P, or Si. Compared to gregoryite and nyerereite, the matrix is richer in silica (490–14,130 ppm Si, average 2,850 ppm), with Si-rich spikes near rapidly quenched sample margins.

Discussion

Mineral/melt partition coefficients

Accurate elemental concentrations in both minerals and the equilibrium liquid are required to calculate partition coefficients. Here, we report elemental concentrations in nyererite, gregoryite, and the groundmass, although no quenched carbonate melt was found. To our knowledge, no glass-forming from quenched carbonatite melt has ever been reported in natural or experimental samples, and all studies using carbonatite melt compositions used the groundmass composition in lieu of glass; we used the same approach herein. To best approach the quenched liquid composition, we averaged 43 LA-ICP-MS groundmass measurements performed with large spot sizes to average the composition of the finely

Fig. 3 Gregoryite, nyerereite, and groundmass compositions measured in this study compared to gregoryite and nyerereite compositions from Mitchell and Kamenetsky (2012, 'M&K12') and Zaitsev et al. (2009, 'Z09')

Fig. 4 Primitive mantle-normalized trace-element concentrations in gregoryite, nyerereite, and groundmass in sample OL_06 from this study, as well as its calculated bulk rock concentrations (2σ errors reported for groundmass), compared to other natrocarbonatite compositions from Oldoinyo Lengai (Keller and Zaitsev 2012, 'K&Z12')
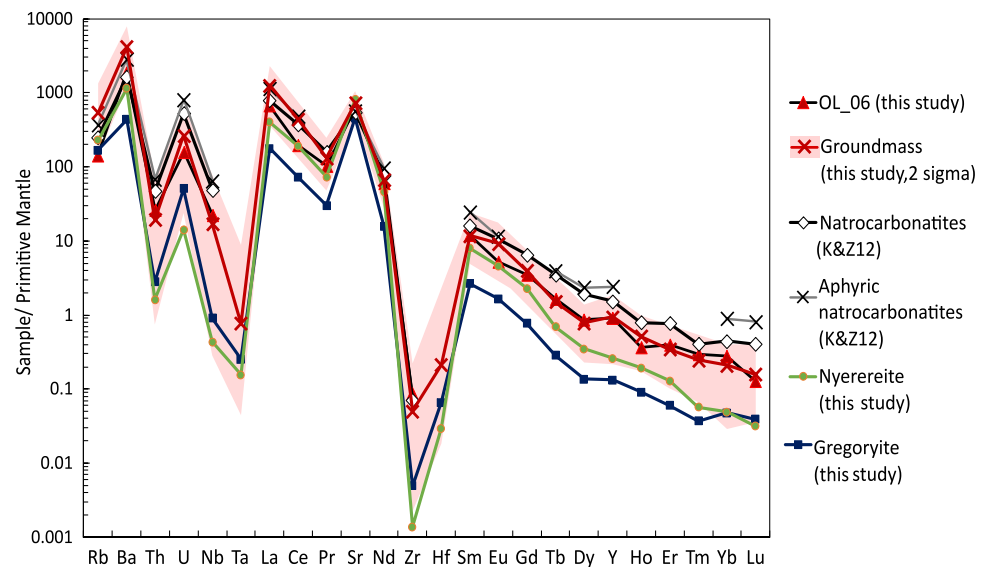
crystallized groundmass. Therefore, we must consider the relative uncertainties on the calculated partition coefficients.

We determined trace-element partition coefficients (*D*) between the groundmass matrix, gregoryite (Ggy), and nyerereite (Nye) for trace elements that are mainly incorporated into the Ca and Na/K sites (Bolotina et al. 2016). Although little information is available on the mineral structure of gregoryite and nyerereite, it is assumed that both the Ca and Na sites are octahedral (VI-fold coordination; McKie and Francis 1977; Bolotina et al. 2016), as are Na sites in natrite (Na_2CO_3) and Na and K sites in $Na_2Mg(CO_3)_2$–$K_2Mg(CO_3)_2$ (Golubkova et al. 2015).

Almost all trace elements are incompatible in both nyerereite and gregoryite: trivalent cations (REEs), Sr, Ba, and Rb have the highest partition coefficients in nyerereite, whereas HFSE partition coefficients are higher in gregoryite. Partition coefficients for LILEs range between 0.1 and 0.9 in both minerals: Sr^{2+} ($D_{Sr}^{Nye} = 0.9$, $D_{Sr}^{Ggy} = 0.5$), Rb^+ ($D_{Rb}^{Nye} = 0.35$, $D_{Rb}^{Ggy} = 0.26$), Li^+ ($D_{Li}^{Nye} = 0.09$, $D_{Li}^{Ggy} = 0.67$), Cs^+ ($D_{Cs}^{Nye} = 0.2$, $D_{Cs}^{Ggy} = 0.2$), and Ba^{2+} ($D_{Ba}^{Nye} = 0.2$, $D_{Ba}^{Ggy} = 0.1$) (Fig. 6; Table 2). Ba and Sr contents increase with Ca content; accordingly, their partition coefficients are higher in nyerereite (CaO = 24 wt.%) than gregoryite (CaO

Table 2 Trace-element concentrations (ppm) in the groundmass of OL_06 and gregoryite (Ggy) and nyerereite (Nye) therein, reported alongside their mineral/melt partition coefficients (D) and uncertainties (σ)

	Groundmass max	Groundmass avg (n=43)	Groundmass 1σ	Ggy avg (n=43)	Ggy 1σ	D Ggy	D Ggy 1σ	Nye avg (n=39)	Nye 1σ	D Nye	D Nye 1σ
Li	1048	451	28.7	304	61.16	0.68	0.19	42.1	4.69	0.09	0.04
Be	30.9	13.7	2.51	1.2	0.33	0.09	0.03	0.55	0.03	0.04	0.02
B	113	68.5	14.13	48.3	15.4	0.70	0.14	66.8	16.17	0.97	0.27
Mg	11,500	5632	230	674	176	0.12	0.03	382	7.05	0.07	0.02
Al	527	58.1	0.57	1.49	0.02	0.03	0.01	3.85	0.08	0.07	0.02
Si	14,130	1657	112	870	14.3	0.52	0.23	404	23.1	0.24	0.15
P	6650	2092	526	11,669	4634	5.58	1.91	1474	453	0.70	0.34
Sc	0.51	0.09	0.011	0.06	0.021	0.73	0.30	0.04	0.006	0.46	0.27
Ti	52.1	14.9	0.61	1.57	0.29	0.11	0.04	1.02	0.03	0.07	0.03
V	1309	515	19.8	107	23.09	0.21	0.06	20.2	0.48	0.04	0.02
Cr	4.19	0.95	0.04	0.94	0.23	0.99	0.38	0.65	0.06	0.69	0.38
Mn	10,665	3472	81.0	1082	237	0.31	0.11	476	21.0	0.14	0.07
Fe	6798	1366	57.2	672	18.42	0.49	0.20	201	5.54	0.15	0.08
Co	0.68	0.16	0.007	0.06	0.09	0.35	0.13	0.04	0.003	0.26	0.14
Ni	0.92	0.26	0.022	0.23	0.04	0.86	0.31	0.10	0.009	0.37	0.19
Zn	376	41.6	3.38	6.26	0.53	0.15	0.07	2.84	0.081	0.07	0.04
Rb	1161	423	8.79	111	26.9	0.26	0.08	146	15.4	0.35	0.16
Sr	30,334	18,714	476	9370	2762	0.50	0.10	17,158	527	0.92	0.25
Y	12.96	5.21	0.12	0.63	0.19	0.12	0.04	1.19	0.036	0.23	0.10
Zr	3.44	0.69	0.01	0.20	0.003	0.29	0.12	0.07	0.003	0.10	0.06
Nb	76.2	14.6	0.39	0.85	0.11	0.06	0.02	0.50	0.008	0.03	0.02
Mo	501	166	4.7	19.0	2.7	0.11	0.04	5.90	0.019	0.04	0.02
Sb	11.9	4.72	0.14	0.35	0.05	0.07	0.02	0.20	0.005	0.04	0.02
Cs	21.1	10.3	0.25	2.10	0.46	0.20	0.05	2.18	0.19	0.21	0.08
Ba	76,157	34,867	1065	3506	942	0.10	0.03	7984	277	0.23	0.09
La	2182	1034	38.6	126	39.4	0.12	0.03	278	17.1	0.27	0.10
Ce	1925	932	33.8	133	42.2	0.14	0.04	338	17.1	0.36	0.13
Pr	95.3	44.2	1.23	8.48	2.76	0.19	0.05	20.2	0.68	0.46	0.17
Nd	210	109	3.41	22.6	7.8	0.21	0.05	63.0	2.08	0.58	0.20
Sm	14.46	6.30	0.19	1.26	0.47	0.20	0.06	3.54	0.12	0.56	0.22
Eu	4.08	1.89	0.07	0.30	0.11	0.16	0.04	0.78	0.042	0.41	0.16
Gd	5.82	2.86	0.12	0.49	0.18	0.17	0.04	1.36	0.055	0.48	0.17
Tb	0.47	0.20	0.009	0.04	0.011	0.19	0.05	0.07	0.006	0.38	0.16

Table 2 (continued)

	Groundmass max	Groundmass avg (n=43)	Groundmass 1σ	Ggy avg (n=43)	Ggy 1σ	D Ggy	D Ggy 1σ	Nye avg (n=39)	Nye 1σ	D Nye	D Nye 1σ
Dy	1.42	0.69	0.03	0.11	0.01	0.16	0.04	0.26	0.012	0.37	0.13
Ho	0.24	0.10	0.005	0.02	0.004	0.16	0.04	0.03	0.003	0.31	0.13
Er	0.48	0.20	0.010	0.03	0.005	0.16	0.05	0.06	0.004	0.31	0.13
Tm	0.06	0.02	0.002	0.004	0.001	0.18	0.06	0.004	0.0007	0.19	0.08
Yb	0.28	0.12	0.01	0.03	0.004	0.21	0.06	0.02	0.003	0.20	0.08
Lu	0.04	0.01	0.002	0.003	0.002	0.21	0.07	0.002	0.001	0.16	0.07
Hf	1.06	0.07	0.005	0.02	0.003	0.28	0.05	0.01	0.002	0.13	0.09
Ta	0.49	0.04	0.001	0.01	0.001	0.29	0.03	0.01	0.001	0.17	0.11
Pb	261	71.4	5.5	11.3	0.75	0.16	0.06	4.14	0.098	0.06	0.03
Th	8.63	2.01	0.12	0.24	0.18	0.12	0.05	0.14	0.004	0.07	0.04
U	21.2	6.77	0.4	1.23	0.058	0.18	0.06	0.35	0.013	0.05	0.02
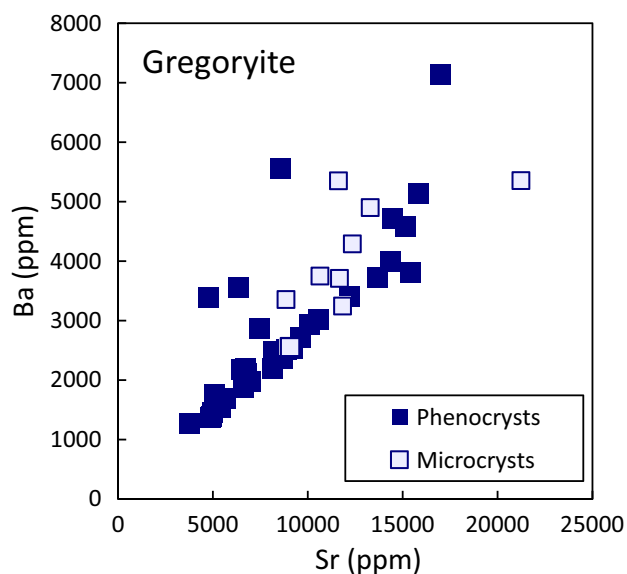
Fig. 5 Sr and Ba concentrations in natural gregoryite phenocrysts and microcrysts from this study (blue and open squares, respectively)

≈ 10 wt.%). Lithium mainly substitutes into the Na site and is more easily incorporated into Na-rich minerals such as gregoryite ($Na_2O \approx 40$ wt.%) compared to nyerereite ($Na_2O \approx 21$ wt.%).

Bivalent transition metals have various D values decreasing from Co^{2+} ($D_{Co}^{Nye} = 0.25$, $D_{Co}^{Ggy} = 0.35$), Mn^{2+} ($D_{Mn}^{Nye} = 0.13$, $D_{Mn}^{Ggy} = 0.3$), Zn^{2+} ($D_{Zn}^{Nye} = 0.06$, $D_{Zn}^{Ggy} = 0.15$), and Mg^{2+} ($D_{Mg}^{Nye} = 0.06$, $D_{Mg}^{Ggy} = 0.12$). REEs behave incompatibly, with Nd having the highest partition coefficients ($D_{Nd}^{Nye} = 0.6$, $D_{Nd}^{Ggy} = 0.2$), and lower D values for LREEs ($D_{La}^{Nye} = 0.27$, $D_{La}^{Ggy} = 0.1$) and HREEs ($D_{Yb}^{Nye} = 0.2$, $D_{Yb}^{Ggy} = 0.2$) (Table 2). REE and Sr partition coefficients have lower to similar values than for calcite in carbonatitic melts ($D_{REE}^{calcite} \approx 1$, $D_{Sr}^{calcite} \approx 1.5$, Chebotarev et al. 2022; $D_{REE}^{calcite} < 0.3$, $D_{Sr}^{calcite} \approx 0.1$, Mollé et al. 2021; Fig. 6). HFSE partition coefficients are low for tetravalent (e.g., $D_{Hf}^{Nye} = 0.13$, $D_{Hf}^{Ggy} = 0.3$) and pentavalent cations ($D_{Nb}^{Nye} = 0.02$, $D_{Nb}^{Ggy} = 0.08$; $D_{Ta}^{Nye} = 0.2$, $D_{Ta}^{Ggy} = 0.3$).

Lattice strain model

Gregoryite–melt and nyerereite–melt partition coefficients (D_i) for elements i of a given valence are correlated to ionic radii and display parabolic distributions, as observed for silicate minerals (e.g., Wood and Blundy 1997; Dalou et al. 2018; Baudouin and France 2019). Lattice strain model (LSM) parameters are only available for carbonates in hydrothermal calcite–fluid experiments (e.g., Voigt et al.

Fig. 6 Trace-element gregoryite/natrocarbonatite melt (blue) and nyerereite/natrocarbonatite melt partition coefficients (green) determined in this study. Calcite/carbonatite partition coefficients from Chebotarev et al. (2022) and Mollé et al. (2021) are shown in gray for comparison. Trace elements are grouped by valence
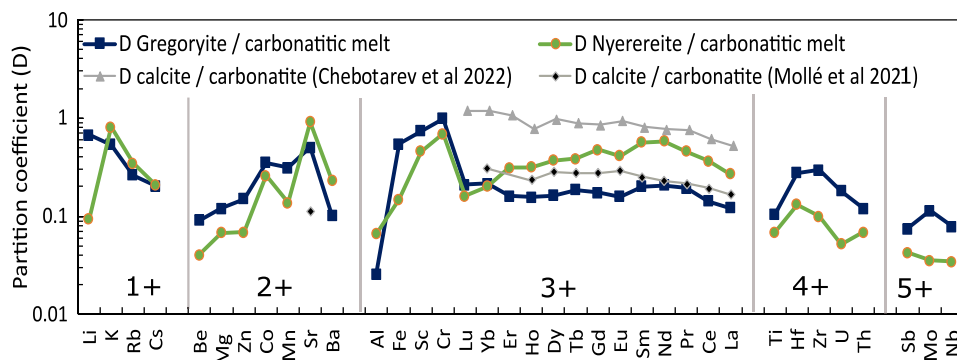
2017; Perry and Gysi 2020). Here, we document the first LSM parameters for carbonates under magmatic conditions.

D_i can be quantified using the classical LSM equation defined by Blundy and Wood (1994) as

$$D_i = D_0 exp\left[\frac{-4\pi EN\left[\frac{r_0}{2}\left(r_i - r_0\right)^2 + \frac{1}{3}\left(r_i - r_0\right)^3\right]}{RT}\right],$$

where D_i is a function of cation radius (r_i in Å), the ideal radius of the crystallographic Ca site occupied by the cations (r_0), the partition coefficient of the ideal cation (D_0) with radius r_0, elastic constant E (Young's modulus), Avogadro's constant N, the universal gas constant R, and temperature T (in Kelvin). We determined the best-fit LSM parameters using the DOUBLE FIT software (Dalou et al. 2018).

Partition coefficients for several isovalent cations are necessary to suitably constrain the LSM parameters. In this study, 2+, 3+, and 4+ partitioning parabolas are well defined, whereas the 1+ and 5+ parabolas are less constrained due to the sparsity of D values for those valences. For all ionic radii, we chose elements to be VI-fold coordinated as proposed for coordination sites for carbonates (e.g., Ca = 1 Å; Na = 1.02 Å).

The gregoryite–natrocarbonatite D_0^{2+} parameter for the Ca²⁺ site is low ($D_0^{2+} = 0.75$), consistent with the incompatible behaviors of all bivalent cations, and r_0^{2+}, is very close to the ionic radius of Ca (1.05 Å). Usually, all rare-earth elements are distributed in the same site and D_{REE} defines a parabolic pattern; here, however, HREEs seem also to be incorporated into the smaller site ($r_0^{3+} = 0.71 \pm 0.01$ Å) as described for some clinopyroxenes and amphiboles in alkaline systems (Baudouin et al. 2020, and references therein). Lu and Tm contents in gregoryite are very low (2–4 ppb Lu, 2–5 ppb Tm) and can be reliable to model HREE distribution is the two sites. However, partition coefficient for Er and Yb are more accurate due to the higher contents of these element in gregoryite (i.e., Yb ~ 30 ± 4 ppb; detection limit at

7 ppb) (see details on supplementary material). With the uncertainties, $D_{Yb}^{Ggy} = 0.21 \pm 0.06$ is close or similar to $D_{Dy}^{Ggy} = 0.16 \pm 0.04$ and $D_{Sm}^{Ggy} = 0.20 \pm 0.06$; consequently, D_{REE} are characterized by a flat pattern (Fig. 6). In the lattice strain model, we propose that REE are incorporated into two sites, with r_0^{3+} around 0.715 Å and 0.97 Å (Fig. 7).

The gregoryite–natrocarbonatite D_0^{3+} parameters for the REE-rich site are very low ($D_0^{3+} = 0.19 \pm 0.02$) and can thus be related to the very high D values of Na and Ca in the carbonatitic liquid. Trivalent cations seem to be distributed into two sites; here, we refer to the smaller (~ 0.71 Å) and larger (~ 0.96 Å) as the "A" and "B" sites, respectively. The LSM parameters obtained for trivalent cations are also characterized by relatively high r_0^B (0.98 ± 0.01 Å) and E^B (318 ± 39 GPa). The LSM parameters for the A site are $D_0^{3+} = 0.75 \pm 0.07$, $E^{3+} = 181 \pm 29$ GPa, and $r_0^{3+} = 0.71 \pm 0.01$ Å (Figs. 7, 8; Table 3). Tetravalent cations, including HFSEs, are incorporated into the A site (i.e., VI-fold coordination), and define a parabolic distribution with $D_0^{4+} = 0.37$, $E^{4+} = 122$ GPa, and $r_0^{4+} = 0.7869$ Å (Table 3).

The nyerereite–natrocarbonatite D_0^{2+} parameter for the Ca²⁺ site is ~ 1 and all bivalent cations' partition coefficients are consistent with a parabolic-partitioning pattern with $r_0^{2+} = 1.12$ Å, which is very close to the ionic radius of Ca (1.05 Å). Trivalent cations are incorporated into two sites with r_0^{3+} of ~ 0.67 Å and ~ 0.97 Å (Fig. 7; Table 3). In contrast to gregoryite, all REEs are incorporated into the larger site with $D_0^{3+} = 0.48$, $E^{3+} = 230$ GPa, and $r_0^{3+} = 0.97$ Å.

The obtained LSM parameters display a strong correlation with valence. The ideal cation radius r_0 decreases significantly with cation charge from $r_0^{1+} = 1.1$–1.2 Å to $r_0^{4+} = 0.75$ Å (Fig. 8; Baudouin and France 2019). Trivalent cations in the B site also show this correlation. The ideal partition coefficient D_0 is dependent on cation charge: D_0 values are the greatest for 1+ cations ($D_0 > 1$) and decrease with increasing charge.

Fig. 7 Trace-element gregory-
ite/natrocarbonatite melt (**a**, **c**,
e) and nyerereite/natrocarbon-
atite melt partition coefficients
(**b**, **d**, **f**) *vs.* ionic radius and
grouped by valence: (**a**, **b**) 2+,
(**c**, **d**) 3+, and (**e**, **f**) 4+. The
best-fit lattice strain model
parameters were determined
using DOUBLE FIT (Dalou
et al. 2018). Two sites were
proposed for trivalent cations
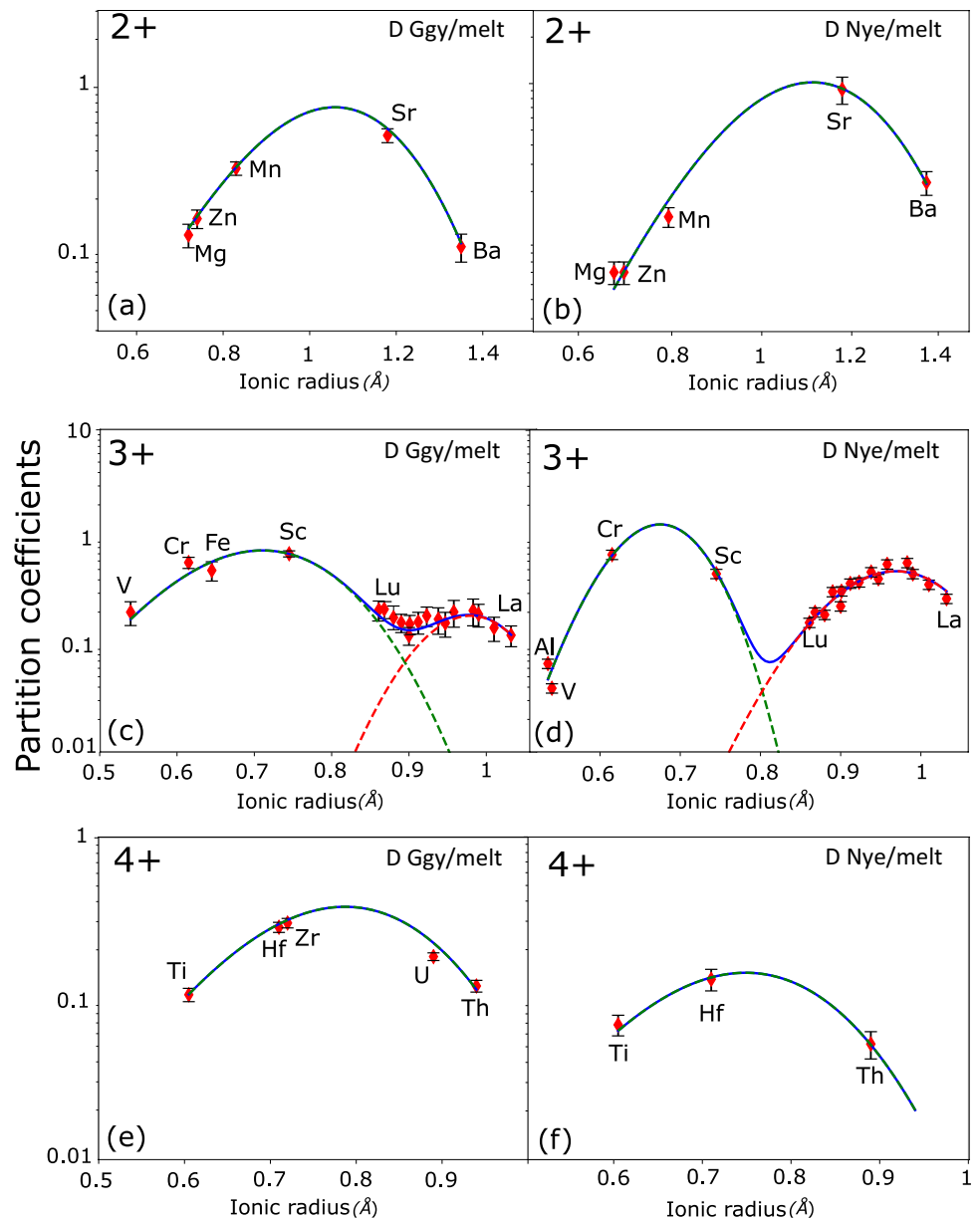
Natrocarbonatite crystallization conditions

Natrocarbonatites are stored at relatively low tempera-
tures and shallow depths beneath OL prior to eruption
($\sim$500–600 °C, $<$100 MPa; Keller and Krafft 1990; Dawson
et al. 1995; Petibon et al. 1998; Kervyn et al. 2008). Crys-
tallization experiments on natrocarbonatites show that both
gregoryite and nyerereite crystallize at low temperatures and
pressures ($<$600 °C, $<$100 MPa; Cooper et al. 1975; Peti-
bon et al. 1998; Mattsson and Caricchi 2009; Mitchell and
Kjarsgaard 2011; Weidendorfer et al. 2017). Specifically,
observations of mineral textures indicate that the natrocar-
bonatitic reservoir beneath OL is at pressure and temperature
conditions that favor the crystallization of nyerereite over
gregoryite ($\sim$100 MPa), whereas gregoryite crystallizes

and nyerereite is resorbed during magma ascent ($<$20 MPa;
Mitchell and Kamenetsky 2008; Zaitsev et al. 2009).

Chemical variations within gregoryite record crystalliza-
tion conditions (Petibon et al. 1998; Mattsson and Caricchi
2009). In sample OL_06, gregoryite phenocrysts contain
8.5–11.0 wt.% CaO and 35–38 wt.% Na_2O, corresponding to
crystallization at 600–560 °C, whereas microcrysts contain
6.9–8.1 wt.% CaO and 39.2–44.0 wt.% Na_2O, correspond-
ing to crystallization at 490–300 °C (at 1 atm; Mattsson and
Caricchi 2009) (Fig. 9). Incompatible trace-element contents
(e.g., Ba, Sr) in gregoryite are higher in low-Ca microcrysts
than in high-Ca phenocrysts phenocrysts (Table 2, Fig. 5).
This evolution is consistent with magmatic differentiation
and can be reproduced by crystallizing 30–35% gregory-
ite without active nyerereite crystallization. Based on our
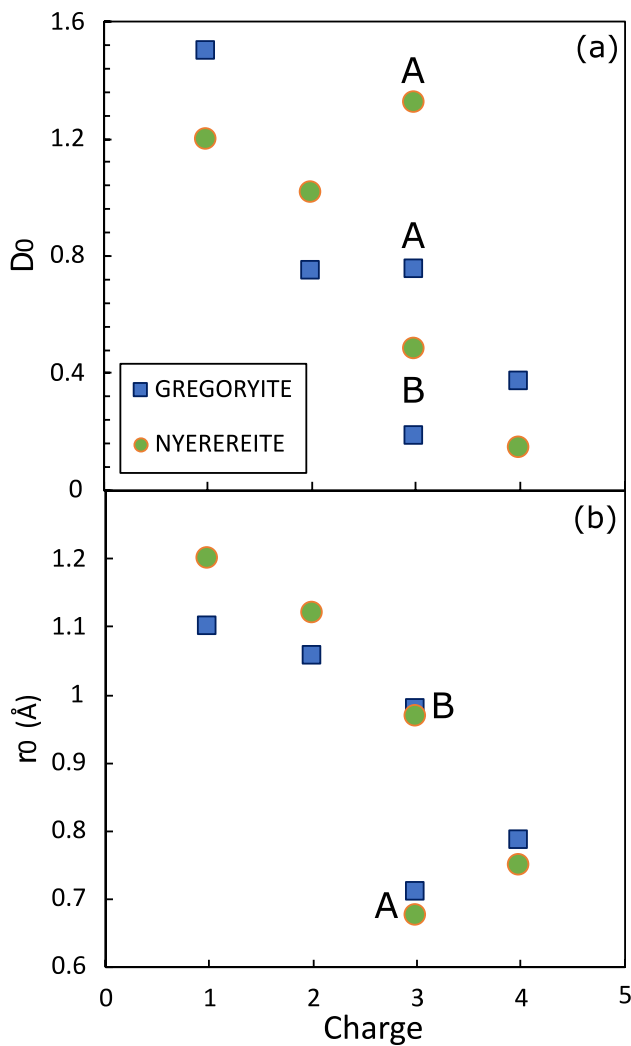
Fig. 8 (**a**) Partition coefficients of the ideal cation (D_0) and (**b**) ideal site radii (r_0) for cations of different valence (1+, 2+, 3+, 4+). Trivalent cations are incorporated into two sites: 'A' and 'B'

results and previous experimental constraints and surface temperature measurements (Krafft and Keller 1989), we propose the following model for the petrogenesis of sample OL_06. Nyerereite and gregoryite phenocrysts began crystallizing within a shallow magmatic reservoir and its related plumbing system (< 3 km depth, 600 °C; Fig. 9). The natrocarbonatite liquid subsequently erupted at the surface and crystallize gregoryite microcrysts down to 300 °C, while nyerereite phenocrysts were partially resorbed (Fig. 9).

Trace-element partitioning and implications for natrocarbonatite evolution

Major-element evolution of carbonatite and natrocarbonatite compositions is likely mainly governed by carbonate mineral crystallization. Because gregoryite and nyerereite are the main minerals in natrocarbonatite, their crystallization controls the melt composition in the different types of natrocarbonatite. The partition coefficients determined herein are thus useful for exploring the parental melt compositions of natrocarbonatites, quantifying the roles of the main phase (gregoryite and nyerereite) during magmatic differentiation, estimating the trace-element contents in associated cumulate assemblages for mineral resource prospecting, and determining the chemical fate of the various types of natrocarbonatite. Based on the partition coefficients, mineral modal proportions, and groundmass composition determined herein, we characterize the major- and trace-element compositions of the parental magma of the 2019 natrocarbonatite sample OL_06 prior to gregoryite and nyerereite crystallization. Ca and Na contents in natrocarbonatitic liquid may been modified by gregoryite and nyerereite crystallization, from the parental liquid containing 17.7 wt.% CaO and 32.6 wt.% Na_2O to aphyric natrocarbonatites composed of 13.2 wt.% CaO and 30.8 wt.% Na_2O (Keller and Zaitsev 2012)(Fig. 2). Gregoryite and nyerereite crystallization had an important

Table 3 Lattice strain parameters for gregoryite and nyerereite in natrocarbonatite OL_06. Two sites ('A' and 'B') were used for trivalent cations

	Gregoryite						Nyerereite					
	D0	σ	E (GPa)	σ	r0 (Å)	σ	D0	σ	E (GPa)	σ	r0 (Å)	σ
2+	0.75	1.16	39	12	1.058	0.006	1.02	0.11	48	3	1.120	0.005
3+A	0.75	0.06	182	29	0.711	0.009	1.32	0.35	624	160	0.675	0.012
3+B	0.19	0.02	318	39	0.980	0.010	0.48	0.04	231	74	0.969	0.026
4+	0.37	1.29	122	100	0.787	0.008	0.14	0.02	131	17	0.749	0.005
	Mollé et al. 2021						Chebatorev et al. 2022					
3+calcite	0.3	0.01	50	5	0.87	0.01	1.2	0.01	75	6	0.85	0.03

Values for trivalent cations in calcite in carbonatite melt are provided for comparison (Mollé et al. 2021; Chebotarev et al. 2022)
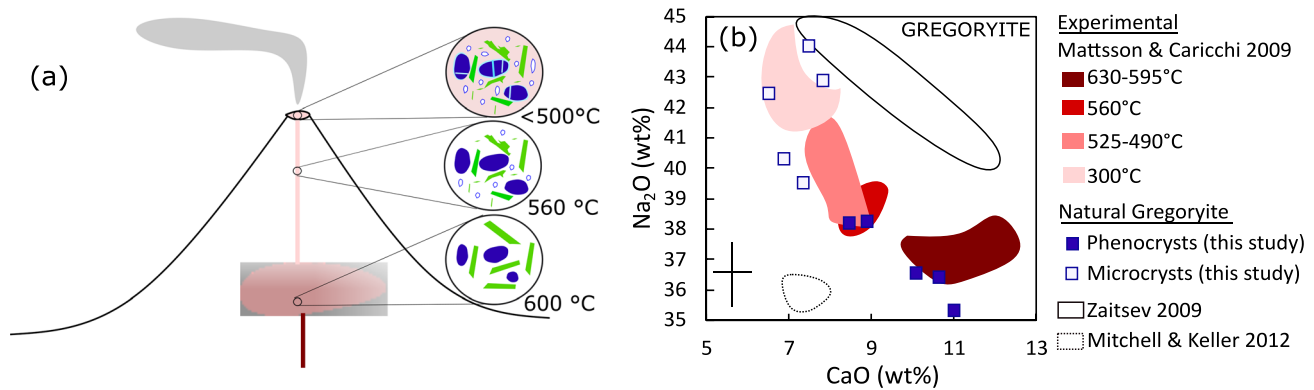
Fig. 9 a Schematic diagram of nyerereite and gregoryite crystallization in natrocarbonatite melt. **b** Variations of the Na$_2$O and CaO concentrations in natural gregoryite phenocrysts and microcrysts from this study (blue and open squares, respectively) and Zaitsev et al. (2009) and Mitchell and Kamenetsky (2012; solid and dashed outlined fields, respectively). Experimental gregoryites from Mattsson and Caricchi (2009) are grouped by crystallization temperature, defining a clear Na$_2$O vs. CaO trend with decreasing temperature. Natural phenocryst and microcrysts correspond to the highest and lowest crystallization temperatures, respectively

impact on the trace-element evolution during differentiation; the calculated parental liquid had 0.5–0.25 × incompatible trace-element concentrations of a type porphyric natrocarbonatite defined by Keller and Zaitsev 2012 (~ 6,000 ppm Sr, 4,000 ppm Ba, 120 ppm Ce, and 3 ppm Nb in the calculated parental melt).

Aphyric natrocarbonatites have been interpreted as evolved natrocarbonatites that represent residual melts after gregoryite and nyerereite crystallization from a type natrocarbonatite (Keller and Krafft 1990). Although this hypothesis can, in theory, be tested using our newly determined partition coefficients, the partition coefficients of gregoryite and nyerereite fall within the same range, making the role of each mineral difficult to decipher. Nonetheless, some specific elemental ratios such as Dy/Yb, V/Y, Ba/Nb, and Ce/Nb evolve differently along the liquid line of descent, because the ratios of the partition coefficient are sufficiently different in each minerals ($D_{Dy}^{Ggy}/D_{Yb}^{Ggy}$ = 0.75 vs. $D_{Dy}^{Nye}/D_{Yb}^{Nye}$ = 1.9; D_V^{Ggy}/D_Y^{Ggy} = 1.7 vs. D_V^{Nye}/D_Y^{Nye} = 0.17; $D_{Ba}^{Ggy}/D_{Nb}^{Ggy}$ = 1.25 vs. $D_{Ba}^{Nye}/D_{Nb}^{Nye}$ = 10; $D_{Ce}^{Ggy}/D_{Nb}^{Ggy}$ = 1.75 vs. $D_{Ce}^{Nye}/D_{Nb}^{Nye}$ = 18.5). These ratios can thus be used to quantify each mineral's involvement during natrocarbonatite fractional crystallization (Figs. 10, 11). Here, we model the differentiation of a type natrocarbonatite through the crystallization of gregoryite and nyerereite using both partition coefficient and elemental ratios (Figs. 10, 11). Chemical characteristics similar to those of aphyric natrocarbonatites are reached after 35–55% crystallization. This is consistent with a major-element mass-balance calculation (50% crystallization; Figs. 10, 11), validating the genetic link between these two types of natrocarbonatite. Elemental ratios, such as Dy/Yb and V/Y, are particularly effective for discriminating the effect of gregoryite vs. nyerereite crystallization, because their partition coefficient ratios are distinct for in each mineral (Fig. 11). Indeed, Dy/Yb increases when only gregoryite crystallizes but decreases when uniquely nyerereite crystallizes or during the crystallization of both nyerereite and gregoryite in equal amounts; the opposite is true for V/Y. During crystallization in the shallow reservoir, which was characterized by both gregoryite and nyerereite crystallization (Fig. 9), the V/Y ratio of the residual melt likely significantly increased, whereas the Dy/Yb, Ba/Nb, and Ce/Nb ratios significantly decreased. However, during the last stage of cooling, which was driven solely by gregoryite crystallization, the Dy/Yb and V/Y ratios of the last remaining natrocarbonatite melt should have slightly increased and decreased, respectively.

Crystallization of accessory minerals, such as sylvite (KCl) and fluorite (CaF$_2$), have a low impact on major-element evolution except for Cl an F but may potentially also play a role in the distribution of trace elements during magmatic differentiation. Using partition coefficient between fluorite and carbonatitic melt (sylvite partition coefficient in not available in literature), a model of fractional crystallization including fluorite has been realized to test the effect of fluorite crystallization during the magmatic differentiation of natrocarbonatites (see supplementary material) (Chebatorev et al. 2019). With extreme values of crystallization for an accessory mineral (~ 20%), we observe a variation of the liquid composition; however, the carbonate minerals remain in control of the trace-element evolution.

Fig. 10 Evolving (**a**) Ba/Nb, (**b**) Dy/Yb, (**c**) Ce/Nb, and (**d**) V/Y elemental ratios in natrocarbonatite melt during fractional crystallization. The compositions of the "type" porphyric natrocarbonatite and aphyric natrocarbonatite are from Keller and Zaitsev (2012). Major-element calculations show that crystallization of 32% gregoryite and 18% nyerereite from the type natrocarbonatite composition can reproduce the aphyric natrocarbonatite composition (50% crystallization is indicated by the gray line). Blue curves represent uniquely gregoryite crystallization, green curves uniquely nyerereite crystallization, and gray curves gregoryite and nyerereite crystallization in equal parts
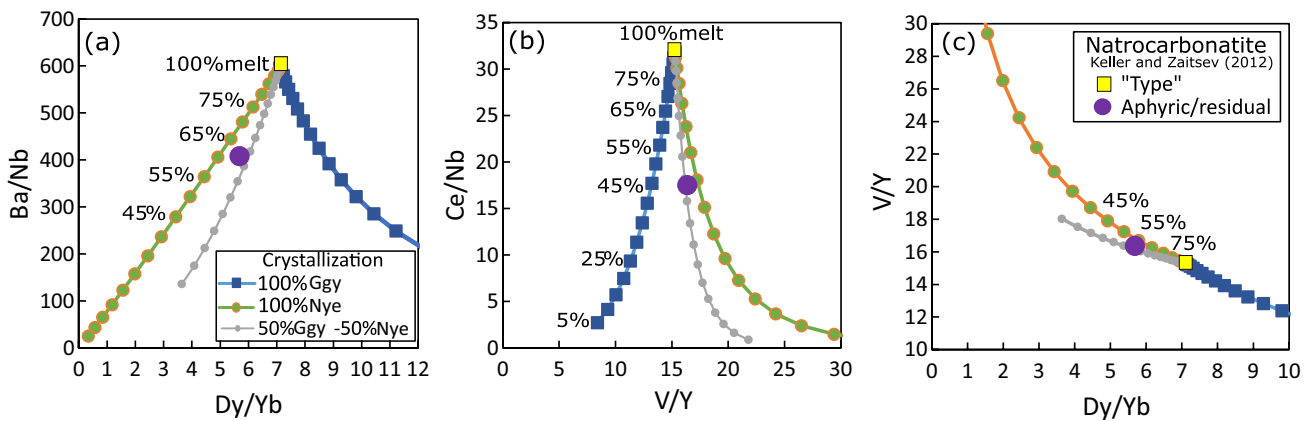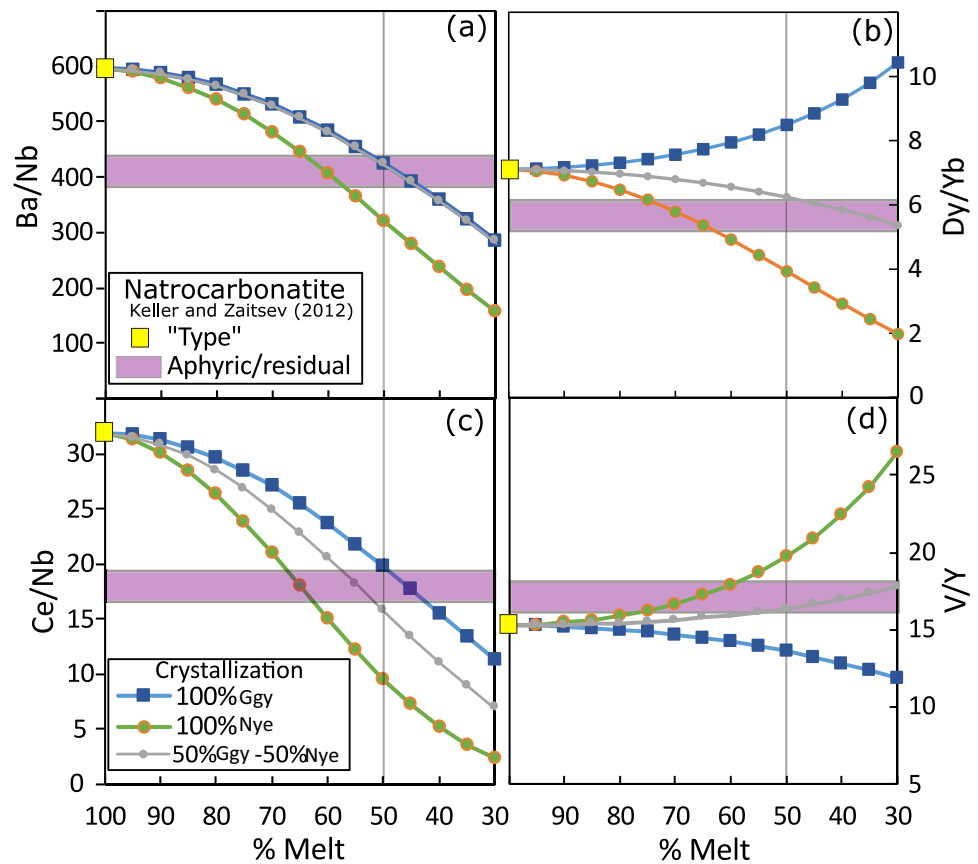
Fig. 11 Evolving (**a**) Ba/Nb vs Dy/Yb, (**b**) Ce/Nb vs V/Y, and (**c**) V/Y vs Dy/Yb, elemental ratios in natrocarbonatite melt during fractional crystallization. The compositions of the "type" porphyritic natrocarbonatite and aphyric natrocarbonatite are from Keller and Zaitsev (2012). Crystallization model is the same as Fig. 10

Conclusions

We determined trace-element partition coefficients between gregoryite, nyerereite, and natrocarbonatite melt at low pressures and temperatures (< 100 MPa, < 600 °C). We fit a lattice strain model to our results to identify that trace elements, such as Ba and Sr, are mainly incorporated into the Ca site with an ideal radius (r_0) that decreases significantly with cation charge from $r_0^{1+} = 1.1$ Å to $r_0^{4+} = 0.75$ Å. All analyzed elements behave incompatibly in the main carbonate minerals in natrocarbonatite, including LILEs (Sr, Ba), REEs (Ce, Nd, Lu), and HFSEs (Nb, Zr). The mineral/melt partition coefficients of several key elements differ between

gregoryite and nyerereite: Nd ($D_{Nd}^{Nye} = 0.6$ *vs.* $D_{Nd}^{Ggy} = 0.2$), Sr ($D_{Sr}^{Nye} = 0.9$ *vs.* $D_{Sr}^{Ggy} = 0.5$), Ba ($D_{Ba}^{Nye} = 0.2$ *vs.* $D_{Ba}^{Ggy} = 0.1$), and Nb ($D_{Nb}^{Nye} = 0.02$ *vs.* $D_{Nb}^{Ggy} = 0.08$). Due to their incompatible behavior, trace-element concentrations increase in the residual liquid during differentiation and crystallization of both gregoryite and nyerereite. The crystallization of gregoryite alone during magma ascent, eruption, and surface cooling increased LREE contents and LREE/HFSE and LILE/HFSE ratios in the last remaining melt.

References

Baudouin C, France L (2019) Trace element partitioning between wollastonite and alkaline silicate magmas. Chem Geol 523:88–94

Baudouin C, France L, Boulanger M, Dalou C, Devidal JL (2020) Trace element partitioning between clinopyroxene and alkaline magmas: parametrization and role of M1 site on HREE enrichment in clinopyroxenes. Contrib Mineral Petrol 175(5):1–15

Blundy J, Wood B (1994) Prediction of crystal–melt partition coefficients from elastic moduli. Nature 372(6505):452–454

Bolotina NB, Gavryushkin PN, Korsakov AV, Rashchenko SV, Seryotkin YV, Golovin AV, Litasov KD (2016) Incommensurately modulated twin structure of nyerereite Na1. 64K0. 36Ca (CO3) 2. Acta Crystallographica Sect B: Struct Sci, Crystal Eng Mat 73(2):276–284

Bosshard-Stadlin SA, Mattsson HB, Keller J (2014) Magma mixing and forced exsolution of CO2 during the explosive 2007–2008 eruption of Oldoinyo Lengai (Tanzania). J VolcanolGeotherm Res 285:229–246

Chebotarev DA, Veksler IV, Wohlgemuth-Ueberwasser C, Doroshkevich AG, Koch-Müller M (2019) Experimental study of trace element distribution between calcite, fluorite and carbonatitic melt in the system CaCO3+ CaF2+ Na2C O3±Ca3(PO4)2 at 100 MPa. Contrib Mineral Petrol 174:1–13

Chebotarev DA, Wohlgemuth-Ueberwasser C, Hou T (2022) Partitioning of REE between calcite and carbonatitic melt containing P S Si at 650–900° C and 100 MPa. Sci Rep 12(1):1–9

Chen W, Kamenetsky VS, Simonetti A (2013) Evidence for the alkaline nature of parental carbonatite melts at Oka complex in Canada. Nat Comm 4(1):1–6

Cooper AF (1975) The system Na2CO3-K2CO3-CaCO3 at 1 kilobar and its significance in carbonatite petrogenesis. Am J Sci 275(5):534–560

Dalou C, Boulon J, Koga KT, Dalou R, Dennen RL (2018) DOUBLE FIT: optimization procedure applied to lattice strain model. Comput Geosci 117:49–56

Dawson S, Smith DE, Ruffman A, Shi S (1996) The diatom biostratigraphy of tsunami sediments: examples from recent and middle Holocene events. Phys Chem Earth 21(1–2):87–92

Dawson JB, Smith JV, Steele IM (1995) Petrology and mineral chemistry of plutonic igneous xenoliths from the carbonatite volcano, Oldoinyo Lengai. Tanzania J Petrol 36(3):797–826

Griffin WL (2008) GLITTER: data reduction software for laser ablation ICP-MS. Laser Ablation ICP-MS in the Earth Sciences: Current practices and outstanding issues 308–311

Golubkova A, Merlini M, Schmidt MW (2015) Crystal structure, high-pressure, and high-temperature behavior of carbonates in the K2Mg (CO3)2–Na2Mg (CO3)2 join. Am Mineral 100(11–12):2458–2467

France L, Brouillet F, Lang S (2021) Early carbonatite magmatism at Oldoinyo Lengai volcano (Tanzania): carbonatite–silicate melt immiscibility in Lengai I melt inclusions. Comptes Rendus Géosci 353(S2):1–16

Keller J, Krafft M (1990) Effusive natrocarbonatite activity of Oldoinyo Lengai, June 1988. Bull Volcanol 52:629–645

Keller J, Spettel B (1995) The trace element composition and petrogenesis of natrocarbonatites. In Carbonatite Volcanism Springer, Berlin, Heidelberg

Keller J, Zaitsev AN (2012) Geochemistry and petrogenetic significance of natrocarbonatites at Oldoinyo Lengai, Tanzania: composition of lavas from 1988 to 2007. Lithos 148:45–53

Keller J, Klaudius J, Kervyn M, Ernst GG, Mattsson HB (2010) Fundamental changes in the activity of the natrocarbonatite volcano Oldoinyo Lengai. Tanzania Bull Volcanol 72(8):893–912

Kervyn M, Ernst GG, Klaudius J, Keller J, Kervyn F, Mattsson HB, Belton F, Mbede E, Jacobs P (2008) Voluminous lava flows at Oldoinyo Lengai in 2006: chronology of events and insights into the shallow magmatic system. Bull Volcanol 70(9):1069–1086

Klaudius J, Keller J (2006) Peralkaline silicate lavas at oldoinyo lengai. Tanzania Lithos 91(1–4):173–190

Krafft M, Keller J (1989) Temperature measurements in carbonatite lava lakes and flows from Oldoinyo Lengai. Tanzania Science 245(4914):168–170

Laxton K (2020) Collection of lava samples from Ol Doinyo Lengai. Nature Rev Earth Environ 1(9):438–438

Laxton K (2022) Natrocarbonatite volcanism at Ol Doinyo Lengai volcano, Tanzania: A multidisciplinary investigation of effusive activity following the 2007–2008 explosive eruption. Thesis publication, University College London

Mattsson HB, Caricchi L (2009) Experimental constraints on the crystallization of natrocarbonatitic lava flows. Bull Volcanol 71(10):1179–1193

McDonough WF, Sun SS (1995) Composition of the Earth. Chemgeol 120:223–253. https://doi.org/10.1016/0009-2541(94)00140-4

McKie D, Frankis EJ, (1977) Nyerereite: a new volcanic carbonate mineral from Oldoinyo Lengai Tanzania. Zeitschrift für Kristallographie-Crystalline Materials 145 (1) 73–95

Mitchell RH (2006) Mineralogy of stalactites formed by subaerial weathering of natrocarbonatite hornitos at Oldoinyo Lengai. Tanzania Mineral Magazine 70(4):437–444

Mitchell RH, Kamenetsky VS (2008) Trace element geochemistry of nyerereite and gregoryite phenocrysts from Oldoinyo Lengai

natrocarbonatite lava. Geochim Cosmochim Acta Supplement 72(12):A637

Mitchell RH, Kamenetsky VS (2012) Trace element geochemistry of nyerereite and gregoryite phenocrysts from natrocarbonatite lava, Oldoinyo Lengai, Tanzania: Implications for magma mixing. Lithos 152:56–65

Mitchell RH, Kjarsgaard BA (2011) Experimental Studies of the System Na_2CO_3–$CaCO_3$–MgF_2 at 0.1 GPa: Implications for the Differentiation and Low-temperature Crystallization of Natrocarbonatite. J Petrol 52 (7–8): 1265–1280

Mollé V, Gaillard F, Nabyl Z, Tuduri J, Di Carlo I, Erdmann S (2021) Crystallisation sequence of a REE-rich carbonate melt: an experimental approach. Comptes Rendus Géoscience 353(S2):217–231

Mollex G, Füri E, Burnard P, Zimmermann L, Chazot G, Kazimoto EO, France L (2018) Tracing helium isotope compositions from mantle source to fumaroles at Oldoinyo Lengai volcano, Tanzania. Chem Geol 480:66–74

Perry E, Gysi AP (2020) Hydrothermal calcite-fluid REE partitioning experiments at 200 °C and saturated water vapor pressure. Geochim Cosmochim Acta 286:177–197

Peterson TD (1990) Petrology and genesis of natrocarbonatite. Contrib MineralPetrol 105:143–155

Petibon CM, Kjarsgaard BA, Jenner A, Jackson SE (1998) Phase relationships of a silicate-bearing natrocarbonatite from Oldoinyo Lengai at 20 and 100 MPa. J Petrol 39:2137–2151

Stoppa F, Jones AP, Sharygin VV (2009) Nyerereite from carbonatite rocks at Vulture volcano: implications for mantle metasomatism and petrogenesis of alkali carbonate melts Research Article. Central Europ J Geosci 1(2):131–151

Voigt M, Mavromatis V, Oelkers EH (2017) The experimental determination of REE partition coefficients in the water-calcite system. Chem Geol 462:30–43

Weidendorfer D, Schmidt MW, Mattsson HB (2017) A common origin of carbonatite magmas. Geology 45(6):507–510

Wood BJ, Blundy JD (1997) A predictive model for rare earth element partitioning between clinopyroxene and anhydrous silicate melt. Contrib Mineral Petrol 129(2):166–181

Yaxley GM, Anenburg M, Tappe S, Decree S, Guzmics T (2022) Carbonatites: classification, sources, evolution, and emplacement. Annu Rev Earth Planet Sci 50:261–293

Zaitsev AN, Keller J (2006) Mineralogical and chemical transformation of Oldoinyo Lengai natrocarbonatites. Tanzania Lithos 91(1–4):191–207

Zaitsev AN, Keller J, Spratt J, Jeffries TE, Sharygin VV (2009) Chemical composition of nyerereite and gregoryite from natrocarbonatites of Oldoinyo Lengai volcano. Tanzania Geology Ore Deposits 51(7):608–616